Bioresource Technology 107 (2012) 411–418

Contents lists available at SciVerse ScienceDirect

Bioresource Technology

journal homepage: www.elsevier.com/locate/biortech

Biomass-based pyrolytic polygeneration system on cotton stalk pyrolysis: Influence of temperature

Yingquan Chen, Haiping Yang *, Xianhua Wang, Shihong Zhang, Hanping Chen

State Key Laboratory of Coal Combustion, Huazhong University of Science and Technology, 1037 Luoyu Road, 430074 Wuhan, PR China

ARTICLE INFO

Article history:
Received 21 August 2011
Received in revised form 20 October 2011
Accepted 21 October 2011
Available online 6 November 2011

Keywords:
Biomass
Polygeneration
Cotton stalk
Product property

ABSTRACT

To study the process of biomass-based pyrolytic polygeneration and its mechanism in depth, the pyrolysis of cotton stalk was investigated in a packed bed, with focus on the evolution of the chemical and physical structures of the solid, liquid and gaseous products. The evolution of product characteristics could be good explaining the process mechanism of biomass pyrolysis. A relationship between the pore distribution of solid products and the fused aromatic rings system revealed by Raman analysis might be exist and need to quantify in further study. Regarding the optimum conditions for obtaining high-quality pyrolytic products from the polygeneration system, the optimum temperature is 550–750 °C, with a higher calorific value of the obtained charcoal (~28 MJ/kg) and a higher surface area (>200 m^2/g). Meanwhile, the calorific value of the gas reaches 8–9 MJ/m^3 and the liquid oil would be used as a platform product in biorefinery.

1. Introduction

How to advance the living standards of the most agriculture-based population in the world is one of the major preoccupations of China government. The abundant resources of biomass have the potential to provide clean energy in rural area, of which crop straw comprises 1.42×10^8 tons of coal equivalents (tce), whereas the forest biomass comprises 2.85×10^8 tce (Yang et al., 2010). However, these abundant biomass resources are improperly utilized. Although 23% of the crop residues are used for forage, 4% for industrial materials, and 0.5% for biogas, large parts are used with lower efficiency or are wasted, with 37% being directly combusted by farmers, 15% being lost during collection, and the remaining 20.5% being discarded or directly burnt in the field (Liu et al., 2008).

In the recent years, the investment on biomass-based power-generation projects has augments by the major electricity-supply enterprises (Zhang et al., 2009), and there are 69 biomass-based direct-combustion power-generation projects (total installed capacity reaches 1424 MW) authorized by the national government and are functioning normally (China, 2010). However, the fact that the biomass is scattered across the land and difficult to collect (Yang et al., 2010) has significantly restricted the scale and economical profitability of biomass-based power-generation plants. Moreover, the electricity generated by the biomass-based power-generation plants does not significantly increase the living standard of farmers.

Gasification of biomass to yield biogas is another popular technology used in the rural areas of China. Altering the pattern of energy usage from firewood to biogas supplied by the gasification station denotes a significant advancement in the living standard for farmers. However, the calorific value of the biogas generated from the current air-gasification technology is 3–5 MJ/m^3, which is not sufficient for the energy requirements of a family. And, the tar generated during air gasification is high, which contaminates the environment. In additional, the economical profitability is lower for the operator of the gasification station because the single product.

Pyrolysis is one of the most promising technologies of biomass utilization, which converts biomass resources to solid char, liquid oil, and biogas. The heating rate and temperature are the most critical parameters in controlling the performance of biomass pyrolysis, particularly with reference to the yield distribution of solid, liquid, and gaseous products (Laird et al., 2009). A flash heating rate and temperatures of 400–600 °C have been shown to provide a high yield of liquid oil (Venderbosch and Prins, 2010). The application of fast pyrolysis for liquid oil production is available presently in China; however, it is unlikely to become a new industry because of the limited application of liquid oil at present. Polygeneration is a promising energy-conversion technology that provides opportunities for high energy-conversion efficiency and economic profitability (Liu et al., 2010; Shangguan et al., 2010). The polygeneration of solid char, liquid oil, and biogas from biomass

---

* Corresponding author. Tel.: +86 027 87542417x8211; fax: +86 027 87545526.
E-mail addresses: chyq721@qq.com (Y. Chen), yhping2002@163.com (H. Yang), wxhwhhy@sina.com (X. Wang), shzhang@mail.hust.edu.cn (S. Zhang), hp.chen@163.com (H. Chen).

0960-8524/$ - see front matter Crown Copyright © 2011 Published by Elsevier Ltd. All rights reserved.
doi:10.1016/j.biortech.2011.10.074

by pyrolysis is a promising biomass-conversion technology because it can effectively advance the biomass-conversion efficiency and provide a higher income from three types of products compared with the system generating a single product, such as liquid oil or biogas, which is available in China. The optimum quality of the three products obtained from biomass-based polygeneration is critical, but there are no details in this context in literature. This article focuses on the characteristics of the products and the mechanism of pyrolysis of a typical agriculture waste, cotton stalk, across a wide range of temperatures, from 250 to 950 °C, to enable the design of a consistent biomass-based polygeneration system.

2. Methods

2.1. Samples

Cotton-stalk samples obtained from WuHan in Hubei province, China, were used in this study. At first, the cotton stalk containing more than 40 wt.% of moisture was dried at 105 °C, crushed, and sieved to obtain a sample of particle size less than 1 mm.

The cotton stalk contained 51.40% of C, 4.00% of H, 43.24% of O, 1.33% of N, and 0.03% of S on a dry ash free basis (daf). Proximate analysis performed on dry sample indicated a quantity of volatile matter of 75.22% and 3.32% of ash, resulting in a fixed carbon amount of 21.46%. The lower heat value of raw cotton stalk (contained 40% of moisture) was 11.629 MJ/kg.

2.2. Pyrolysis experiment

The pyrolysis of cotton stalk was carried out in a fixed-bed reactor. There are three essential parts for the reactor system: a vertical stainless steel tube (height = 600 mm, internal diameter = 38 mm) with a moving silica sample-carrier (the preheated gas current can penetrate into the carrier through the gas-distribution frit); a ice cooling system collecting the condensable volatiles (liquid product); and a gas cleaning–drying system collecting the gas product. For each trial, about 3 g of sample was loaded into the sample carrier. A flow of preheated nitrogen (99.99%, 1 L/min) was used to provide a reductive atmosphere in the reactor.

When pyrolyzing the cotton stalks, the reactor was pre-heated to the experimental temperature. The sample carrier was moved rapidly from the top to the heated zone of the reactor. The samples were retained for about 30 min to ensure no volatiles remained. A range of temperatures, from 250 °C to 950 °C, was investigated. After each trial, the reacted sample (solid product) was cooled with the reactor to the ambient environment, and then was weighed and recorded as the solid charcoal yield. Gaseous yield was calculated by combining the volumes of all the gases collected during pyrolysis. The liquid product consisted of bio-oil, water, and some fine particles, and its yield was obtained by calculating the increase in weight of the condenser system. Each test experiment was carried out three times, and the repeatability was very good. All the data provided for the product yield were the average value of three trials. The analysis of products obtained in each trial was carried out according to the following method, and the final result was the average value.

2.3. Analysis of gas and liquid oil

A dual-channel micro-GC system (Micro-GC 3000A, Agilent Technologies, USA), equipped with thermal conductivity detectors, was used to analyze qualitatively and quantitatively the gaseous components of biomass pyrolysis. The details of the analysis methods have been described elsewhere (Yang et al., 2006a).

The water content of liquid oil was measured by Karl–Fischer titration (TitroLine KF-10, SCHOTT, Germany) according to the ASTM D 1744 protocol prescribed by the American Society for Testing and Materials (titrant: Hydranal composite 2, Metrohm 787 KFTitrino).

The main components of the bio-oil were specified in detail using gas chromatography–mass spectroscopy (GC–MS; HP7890 series GC with an HP5975 MSdetector) equipped with a capillary column (Agilent: HP-5MS, 19091S-433; length, 30 m; internal diameter, 250 μm; film thickness, 0.25 μm). The film in the column was formed of bonded 5% phenyl and 95% methyl siloxane. The GC oven temperature was initiated at 40 °C for 1 min, which then reached 300 °C in three steps: 10 °C/min to 100 °C for 0 min, 5 °C/min to 200 °C for 0 min, and 20 °C/min to 300 °C for 3 min. The injector temperature was 250 °C, and the split ratio was 20:1. In each trial, 1 μL of the sample was injected. The flow rate of the carrier gas (Helium) for the column was 1.0 ml/min. After 2 min of solvent delay, the sample was directly introduced into the ion source of a Hewlett–Packard model 5975 series mass-selective detector operated in an electron-impact ionization mode and scanned over an m/z range of 30–500. The software GG1034C Chemstation, with a National Bureau of Standards library, was used to identify each compound based on the retention time and the matching mass spectrum of the standards in the spectral library. All components were semi-quantified using an internal standard of 0.2 mass % of phenanthrene in methanol containing 5 mass % of liquid oil. A microfilter (0.45 μm) was used to remove the particles in the liquid oil before injecting into the GC–MS. The analysis of liquid product was carried out rapidly to ensure the composition unchanged.

2.4. Analysis of solid charcoal

Proximate analyses of solid charcoals were conducted using ASTM standards to obtain moisture content, volatiles, fixed carbon, and ash content. Ultimate analyses of the dried samples for carbon, hydrogen, nitrogen, and sulfur were carried out with a CHNS/O elementary analyzer (Vario Micro cube, Germany). The calorimetric values of the dried samples were measured by bomb calorimetry (Parr 6300, USA).

The isothermal adsorption of nitrogen at 77 K was studied using an automatic adsorption equipment (Micromeritics, ASAP 2020, USA) to analyze the pore-structure characteristics of the solid charcoals. Before the adsorption measurements, the sample was degassed at 150 °C under a vacuum (pressure of 50 μm Hg) for 10 h. To obtain the information related to micropore structure, a relatively lower adsorption pressure of 10^{-6} were applied (P/P_0), and the N_2-adsorption isotherm was obtained at relative pressures (P/P_0) ranging from 10^{-6} to 0.995. The BET surface area (S_{BET}), micropore surface area (S_{mic}) and micropore volume (V_{mic}), total volume (V) of the solid products at varied temperatures were determined by application of the Brunauer–Emmett–Teller (BET) equation, *t*-plot method and single point adsorption total pore volume analysis, respectively (Fu et al., 2009b; Ismadji et al., 2005). The pore-size distribution was analyzed by the density-function theory (DFT) method, which can be used to calculate the distribution of micro-, meso-, and macropores, simultaneously (Feng and Bhatia, 2003; Ismadji et al., 2005).

The infrared spectrum of solid charcoals between 4000 and 400 cm^{-1} was recorded using a VERTEX 70 spectrometer (Bruker, Germany). Each spectrum is the result of 120 accumulated scans with 4 cm^{-1} resolution, and the apodization function was the Happ–Genzel type. To prepare the pellet, approximately 0.7 mg of dried solid sample and 70 mg KBr (Merck, spectroscopy grade) were mixed, and the resulting mixture was pressed successively at pressures of 5 tons/cm^2 for 5 min and 10 tons/cm^2 for 5 min under vacuum.

The Fourier transform–Raman (FT–Raman) spectra obtained using a Bruker's VERTEX-70 Series Fourier transform infrared (FTIR) spectrometer was used to characterize the structure of the samples, following the procedure of Keown et al. (2008) and Li et al. (2006). The light source for Raman spectroscopy was a Nd:YAG laser at 1064 nm, and the Raman spectra were collected using an InGaAs detector at room temperature. Laser power of 250 mW was used, and every spectrum represented the average of 80 scans. The Raman spectra in the range between 800 and 1800 cm^{-1} were curve-fitted by the Opus software (version 6.00) with 10 Gaussian bands, as recommended by Keown et al. (2008) and Li et al. (2006). The 10 Gaussian bands shown in Table 1 represent some typical structures. The chars were ground and diluted to 0.5 wt.% with spectroscopic grade KBr.

The X-ray diffraction (XRD, PANalytical B.V., X'Pert PRO, The Netherlands) for the crystal structure of solid products also was carried out to provide more information of solid chars during pyrolysis.

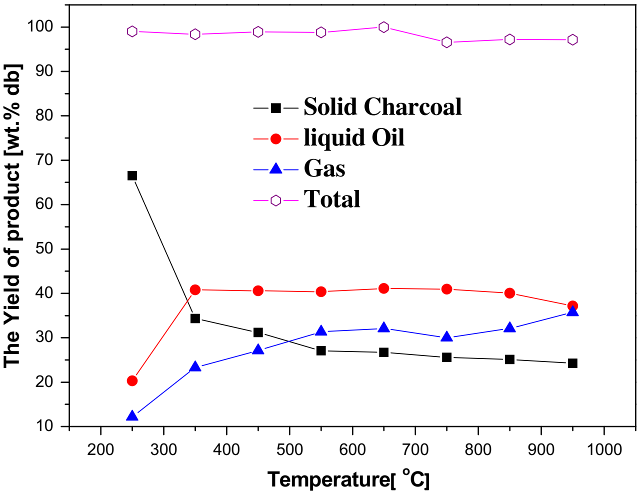

Fig. 1. The yield distribution of cotton stalk pyrolysis at different temperature.

3. Result and discussion

3.1. Product-distribution property

The yield distributions of solid charcoal, liquid oil, and gaseous product from cotton-stalk pyrolysis at different temperatures (250, 350, . . . , 850, and 950 °C) are shown in Fig. 1. The charcoal content was reduced greatly, from 66.5 to 26.73 wt.%, as the temperature increased from 250 to 650 °C. After that, with further increase in temperature from 650 to 950 °C, almost no significant changes were observed in the charcoal yield. The devolatilization of cotton stalk was concentrated at lower temperatures (250–650 °C). Charcoal is an important product of biomass-based polygeneration, which can significantly advance the economical profitability of the polygeneration system for the operator. Gas yields also increased greatly with an increase in temperature from 250 to 550 °C; then, with further increase in temperature, the increasing extent of gas yield was lowered, reaching its maximum value (35.71 wt.%) at 950 °C. Gas is another important product in the biomass-based polygeneration system, which is provided indirectly as the fuel to the residents around the polygeneration station. A high yield and quality of the gaseous product is in the interest of both farmers and local government. However, a high operating temperature is needed, which augments the cost of the system. In terms of the liquid part, the liquid yield comprised 40 wt.% of the mass of the biomass sample and showed a slight increase with temperatures greater than 250 °C.

Table 1

Summary of Raman peak/band assignment representing the typical structures.

Band name	Band position (cm^{-1})	Description	Bond type
G_l	1700	Carbonyl group C=O	sp^2
G	1590	Graphite E_{2g}^2;aromatic ring quadrant breathing; alkene C=C	sp^2
G_r	1540	Aromatics with 3–5 rings; amorphous carbon structures	sp^2
V_l	1465	Methylene or methyl; semicircle breathing of aromatic rings; amorphous carbon structures	sp^2, sp^3
V_r	1380	Methyl group; semicircle breathing of aromatic rings; amorphous carbon structures	sp^2, sp^3
D	1300	D band on highly ordered carbonaceous materials; C–C between aromatic rings and aromatics with not less than 6 rings	sp^2
S_l	1230	Aryl–alkyl ether; para-aromatics	sp^2, sp^3
S	1185	$C_{aromatic}$–C_{alkyl}; aromatic (aliphatic) ethers; C–C on hydro-aromatic rings; hexagonal diamond carbon sp^3; C–H on aromatic rings	sp^2, sp^3
S_r	1060	C–H on aromatic rings; benzene (ortho-disubstituted) rings	sp^2
R	960–800	C–C on alkanes and cyclic alkanes; C–H on aromatic rings	sp^2, sp^3

3.2. Properties of gaseous product

The accumulated amounts of the four major gases released—H_2, CO, CO_2, and CH_4—are represented in moles per unit biomass in Fig. 2. Although three types of incondensable light hydrocarbons, C_2H_6, C_2H_4, and C_3H_8 were detected, the total amounts of these light hydrocarbons was less than 0.5% of the volume of the gaseous product. At the onset temperature of 250 °C, CO_2 and CO were released more rapidly than the other gases. On further increasing the temperature, the amount of CO_2 released remained almost unchanged even at temperatures above 350 °C. Some previous researchers have confirmed that CO_2 is the major gas generated during the low-temperature decarboxylation of hemicellulose and cellulose found in biomass (Mahinpey et al., 2009; Shen and

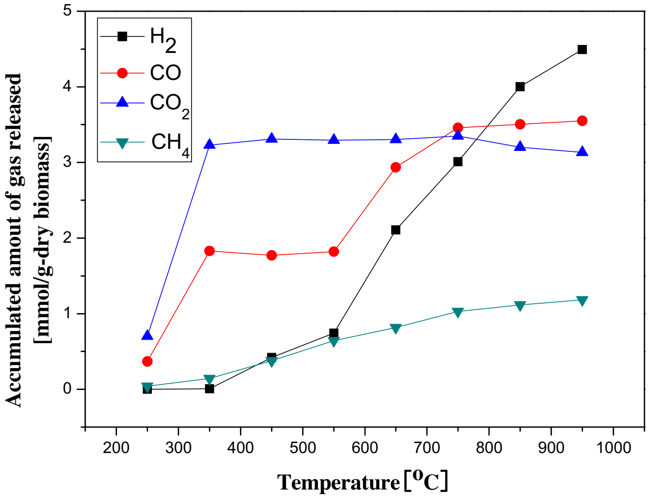

Fig. 2. The accumulated amount of gas released at different pyrolysis temperatures.

Table 2
Gas product composition and low heat value (mol% N_2-free and H_2O-free) at different temperature.

Temperature	250	350	450	550	650	750	850	950
Gas product composition (vol.%)								
H_2	0.02	0.13	6.72	12.17	22.16	27.74	35.66	36.33
CH_4	3.81	2.75	6.00	10.52	8.57	9.50	9.93	9.58
CO	32.99	35.11	28.19	29.86	30.85	31.89	25.89	28.73
CO_2	63.17	62.01	59.08	47.46	38.41	30.87	28.52	25.36
LHV (MJ/m^3)	5.54	5.44	6.44	8.86	9.37	10.43	10.68	10.99

Gu, 2009; Yang et al., 2006a). However, another notable release of CO occurs at 550–750 °C, which may be generated during the decarbonylation process in the aromatic condensation of lignin (Fu et al., 2009a). Before the temperature reaches 450 °C, no H_2 was released; however, a conspicuous release of H_2 occurred after 550 °C. Aromatic condensation and thermal cracking of heavy hydrocarbons contributed to the release of H_2 (Yang et al., 2006a). Moreover, CH_4 behaved similar to H_2, but the released amount was far lower than that of H_2. The result of the gas releasing is same to several previous studies (Duman et al., 2011; Fu et al., 2011; Mahinpey et al., 2009)

For the success of the biomass-based polygeneration system, a high quality of the evolved gas, such as consistent composition and higher calorific value, is an important operating objective. Table 2 shows the composition of the gas and the low calorific value (mol%, N_2-free) of the products at different temperatures. On increasing the temperature, the proportion of H_2 and CH_4 in the gas increased, which are the major contributors of calorific value; thus, the low calorific value of the gas showed an increase. However, at temperatures above 750 °C, the increase in the calorific value of gas ceased, which indicates that operation at high temperatures could not be economical. The optimal operating temperature for polygeneration may be 550–650 °C, but the proportion of CO_2 not undergoing combustion was very high, reaching approximately half of the gas volume. Therefore, abstraction of CO_2 from the gas is needed. If the proportion of CO_2 decreased to 10%, the calorific value would increase from 8–10 MJ/m^3 to 13–15 MJ/m^3. Some reports suggest that the char obtained from biomass have the capacity to adsorb CO_2; hence, future research work will investigate the CO_2-adsorptioncapacity of char obtained from the biomass-based polygeneration system to improve the quality of the gaseous product.

3.3. Properties of liquid oil

Table 3 shows the composition of liquid-oil by GC/MS. The water content, as quantified by the Karl–Fischer titration, reached 67–75 mass % of the liquid oil. The compounds identified by GC–MS accounted for 20–29 mass % of the oils. The chemical compounds identified mainly consisted of carboxylic acids, furans, ketones, esters, cyclopentenes, and phenols. Fig. 3 shows the accumulated amount of grouping composition in liquid oil at varied temperatures. The composition of liquid oil is complicated, however, several researchers suggest that phenols is mainly from the degradation of lignin while carboxylic acids, furans, ketones, and cyclopentenes are from the degradation of cellulose and hemicellulose (Ayhan, 2007; Duman et al., 2011; Wang et al., 2011).

The liquid oil obtained at 250 °C contained acids, furans, and ketones, with only a slight amount of phenols. At this low temperature, the major component degraded was hemicellulose, composed of various polymerized monosaccharides, such as allose, altrose, mannose, galactose, xylose, alucuronic acid, and galacturonic acid (Wang et al., 2009; Yang et al., 2006b). On increasing the temperature, the derivatives of cyclopentene and phenol were formed. The derivatives of cyclopentene may be generated form the degradation of cellulose, composed of polymerized glucose; and the derivatives of phenol may be mostly from the degradation of lignin (Shen and Gu, 2009; Wang et al., 2009). The maximum amounts of organic composition was obtained at 450–650 °C, but decreased above 750 °C. It may be attributed to the secondary reactions of tar at high temperature (>700 °C) (Bahng et al., 2009) and it is difficult to identify the secondary reaction in the role of the pyrolysis process since the intermediates

Table 3
Composition of liquid-oil determined by GC/MS (mass % of liquid-oil).

No.	Compound	RT (min)	Temperature							
			250	350	450	550	650	750	850	950
0	Water		74.69	70.51	66.70	68.16	67.50	69.39	73.74	74.09
1	Formic acid	2.7	1.35	0.93	1.03	0.98	1.03	0.84	0.66	0.60
2	Acetic acid	3.2	8.41	10.27	9.82	9.67	9.54	8.59	7.67	6.95
3	2-Propanone,1-hydroxy-	3.4	1.08	1.51	1.75	1.78	1.71	1.65	1.23	1.39
4	Acetic acid, hydroxy-, methyl ester	3.6	0.22	0.24	0.33	0.38	0.32	0.29	0.17	0.12
5	1-Hydroxy-2-butanone	4.2	0.52	0.67	0.78	0.79	0.67	0.61	0.50	0.47
6	Furfural	4.6	0.51	0.78	0.87	0.92	0.79	0.62	0.54	0.53
7	Pyridine,2-methyl-	4.8	0.00	0.15	0.20	0.19	0.19	0.23	0.18	0.14
8	2-Furanmethanol	5.3	1.09	1.33	1.25	1.10	0.98	0.84	0.68	0.61
9	2-Propanone,1-(acetyloxy)-	5.4	0.27	0.44	0.50	0.45	0.40	0.39	0.31	0.28
10	2(5H)-Furanone	6.2	0.30	0.60	0.62	0.64	0.58	0.56	0.46	0.46
11	2-Cyclopenten-1-one,2-hydroxy-	6.4	0.00	0.40	0.43	0.45	0.41	0.31	0.32	0.32
12	2-Cyclopenten-1-one,3-methyl-	6.9	0.00	0.00	0.17	0.15	0.17	0.20	0.14	0.15
13	Phenol	7.2	0.00	0.15	0.27	0.27	0.28	0.26	0.24	0.34
14	Phenol,2-methyl-	8.4	0.01	0.88	0.92	1.09	0.88	0.79	0.74	0.68
15	Phenol,4-methyl-	8.7	0.01	0.21	0.26	0.26	0.29	0.32	0.24	0.30
16	Phenol,4-methoxy-	8.9	0.02	0.76	0.83	1.55	1.41	1.28	1.10	1.06
17	1,3-Propanediamine,N-methyl-	9.3	2.28	2.04	1.79	1.75	1.62	1.55	1.07	1.06
18	2-Cyclopenten-1-one,3-ethyl-2-hydroxy-	9.6	0.20	0.37	0.48	0.32	0.33	0.32	0.17	0.24
19	Phenol,2-methoxy-4-methyl-	11.0	0.01	0.26	0.28	0.19	0.25	0.31	0.14	0.13
20	1,2-Benzenediol	11.6	0.02	0.91	1.26	1.34	1.61	1.93	1.58	1.44
21	1,2-Benzenediol,3-methoxy-	12.7	0.03	0.47	0.56	0.66	0.55	0.31	0.51	0.47
22	2-Methoxy-4-vinylphenol	13.7	0.14	0.64	0.38	0.30	0.30	0.29	0.59	0.20
23	Phenol,2,6-dimethoxy-	14.6	0.09	0.83	1.14	1.15	1.35	1.54	1.57	1.66
24	Benzoic acid,4-hydroxy-3-methoxy-	16.8	0.03	0.71	0.69	0.49	0.50	0.39	0.28	0.29
25	5-tert-Butyl pyrogallol	18.6	0.06	0.39	0.41	0.32	0.32	0.31	0.28	0.18
26	Phenol,2,6-dimethoxy-4-(2-propenyl)-	22.4	0.03	0.58	0.38	0.33	0.28	0.17	0.25	0.16
27	Desaspidinol	24.0	0.04	0.16	0.38	0.42	0.42	0.32	0.38	0.24

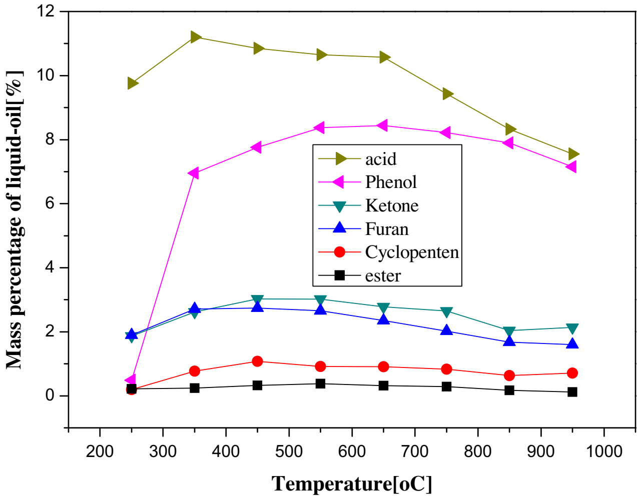

Fig. 3. The accumulated amount of grouping composition in liquid oil at varied pyrolysis temperatures.

cannot be observed. Vamvuka and Sfakiotakis (2011) suggest that the degradation reaction of biomass is a parallel reaction of the first-order degradation reaction of cellulose, hemicellulose and lignin, and the releasing of phenols was consistent with Vamvuka and Sfakiotakis' conclusion, however, the diethoxytetrahydrofuran from degradation of cellulose (Wang et al., 2011) was not observed in the liquid oil. Therefore, the releasing of composition in liquid oil is difficult to identify the pyrolysis mechanism in depth.

Acetic acid was the major component of liquid oil, and its yield from fast pyrolysis is higher than the yield from slow pyrolysis (Bahng et al., 2009; Duman et al., 2011). In this study, the yield of acetic acid obtained before 650 °C was consistent with previous studies (Duman et al., 2011; Sevgi, 2003). The breaking of the acetyl groups of hemicellulose and cellulose is contributed to the generation of acetic acid (Wang et al., 2009). The increase in yield of acetic acid between 250 and 350 °C might be caused by the degradation of cellulose because the polymerized structure of cellulose is destroyed at temperatures above 300 °C (Wang et al., 2009). However the yield of acetic acid was notably decreased at higher temperatures (>650 °C). It may be due to the secondary degradation of acetic acid in the reactor at high temperature since acetic acid is a thermally unstable product (Demiral and Ayan, 2011; Mahinpey et al., 2009)

In this study, the pyrolysis conditions were different from those in fast pyrolysis, which indicates that the species of chemical compounds in the liquid oil are not as complicated as those in the bio-oil obtained from fast pyrolysis (Duman et al., 2011). Although the yield of liquid product is inevitable in the biomass-based polygeneration system, the types of chemical compounds obtained are not too complicated, and the generation of heavy compounds is controlled (Sevgi, 2003), which decreases the contamination of the environment in the rural areas, in contrast to the situation with an air-gasification station. Liquid oil can be used as an important chemical material; however, the total amount is very little and insufficient for feeding a manufacturing unit. Nevertheless, the interest in the gaseous and char products can spread the utilization of the biomass-based polygeneration technology; consequently, a new liquid oil-treating manufacturing process should be designed to tackle the potential huge amounts of oils.

3.4. Properties of solid charcoal

The properties of the chars are listed in Table 4. In ultimate analyses, with an increase in the pyrolysis temperature from 250 to 950 °C, the carbon content of the chars increased from 59.56 to 92.85 wt.%; however, the hydrogen content decreased from 5.70 to 0.63 wt.%, and the oxygen content also showed a similar trend, decreasing from 33.66 to 5.24 wt.%. This observation indicates that increasing the pyrolysis temperature increases the degree of carbonization of the chars. In proximate analyses, the volatile content decreased significantly with increase in temperature from 250 to 750 °C, whereas no obvious change was observed at temperatures >750 °C. In addition, the calorific value of the chars almost remained invariant. These results is similar with previous researches (Fu et al., 2011; Sevgi, 2003; Yao et al., 2011)

The evolution of the structure of solid charcoal at different temperatures could effectively explain the mechanism of pyrolysis. This study not only concerns the properties of the products, but also expects to find the details of the mechanism of cotton-stalk pyrolysis. Therefore, several methods, such as FTIR spectroscopy, FT–Raman spectroscopy, and pore-distribution analysis, were carried out to analyze the evolution of the structure of solid charcoal.

The result of the FTIR spectra shown that the raw cotton-stalk sample had the most complex transmittance bands, and the char obtained at 250 °C was similar to the raw sample; however, several functional groups vanished. On increasing the temperature above 250 °C, the chars became substantially different in terms of the IR spectra. At high temperatures, there were almost no functional groups in the chars; but the amorphous carbon structure absorbed the IR light, which is attributed to the slant of the IR spectrum. A broad band at 3406–3388 cm^{-1} is due to the stretching of the hydrogen-bonded OH group. This peak diminished sharply to zero when the temperature was increased to 450 °C, which might be attributed to the dehydration of the biomass, because a large amount of water was released simultaneously. The bands attributable to aliphatic CH_n (2945–2916 cm^{-1}) and aromatic CH_3 (2843–2841 cm^{-1}) also decreased to zero as the temperature increased to 450 °C, possibly due to the breaking of the weak bonds between the C and the H of the alkyl groups. The breaking of the –C–H functional groups brought about the release of CH_4, C_2H_6, and C_2H_4 and resulted in the presence of CH_4 and C_2-hydrocarbons in the gaseous products (refer to Fig. 2). The bands arising from the stretching of the C=O group (1720 cm^{-1}) and the C–O–C or C–O group (1090 cm^{-1}) showed a striking decrease in intensity in the chars obtained at 250 and 350 °C compared to those of raw cotton, which is in good agreement with the observation that CO and CO_2 evolved violently between 250 and 350 °C (as shown in Fig. 2). On the contrary, the aromatic skeletal vibration (1662–1587 and 1429–1417 cm^{-1}) and aromatic C–H deformation (816 and 781 cm^{-1}) increased, compared to raw cotton stalk, when the cotton stalk was pyrolyzed at 350 °C, with these peaks showing maximal intensities at 450 °C. A decrease of these bands at higher temperatures reflected the carbonization resulting from cracking and the rebuilding of aromatic rings, releasing a significant amount of H_2 (Fig. 2). As the final temperature increased to 850–950 °C, almost no organic functional groups remained in the solid charcoal residue.

FTIR spectroscopy and Raman spectroscopy can provide information on the surface and bulk chemical structures because chemical bonds have absorptions at characteristic frequencies in the infrared region of light. However, compared with FTIR spectroscopy, FT–Raman spectroscopy can effectively bring out the structural features of highly disordered carbonaceous materials, such as chars (Bahng et al., 2009). The Raman peak areas and the band ratios can show the evolution of the structural features during pyrolysis. FT–Raman spectra were not obtained for the char pyrolysis carried out at 250 and 350 °C, probably because microcrystalline graphite was not generated and could not induce the inelastic scattering of incident photons. With increase of the pyrolysis temperature, the total Raman intensity decreased due to the loss

Table 4
The basic analysis of chars at different temperature.

Temperature	250	350	450	550	650	750	850	950
Ultimate analysis (daf, wt.%)								
C	59.56	77.55	86.10	90.26	91.62	91.88	92.14	92.85
H	5.70	4.19	3.03	2.14	1.19	1.20	0.86	0.63
N	1.00	1.41	1.33	1.31	1.17	1.31	1.00	0.87
S	0.08	0.12	0.15	0.17	0.18	0.22	0.34	0.42
O	33.66	16.74	9.40	6.12	5.84	5.39	5.66	5.24
Proximate analysis (d, wt.%)								
Volatile	43.91	26.81	18.85	13.11	9.51	7.90	7.90	7.42
Ash	3.65	6.35	7.56	8.42	8.33	7.95	8.36	8.39
Fixed carbon	52.44	66.84	73.59	78.48	82.16	84.15	83.74	84.19
LHV(MJ/kg)	20.53	25.70	27.63	28.18	27.84	27.97	27.49	27.41

Table 5
Characteristics of porosity in the chars.

Samples	S_{BET} (m^2/g)	Surface area of micropore S_{mic} (m^2/g)	Total pore volume V (10^3 ml/g)	Pore volume of micropore V_{mic} (10^3 ml/g)
Raw	2.19 ± 0.41	0.36 ± 0.12	0.105 ± 0.029	0.001 ± 0.000
250	3.02 ± 0.52	0.81 ± 0.26	0.120 ± 0.033	0.003 ± 0.001
350	4.27 ± 0.81	1.70 ± 0.32	0.084 ± 0.021	0.007 ± 0.002
450	7.96 ± 0.68	2.19 ± 0.44	0.140 ± 0.047	0.009 ± 0.003
550	122.92 ± 8.94	87.46 ± 6.26	0.683 ± 0.061	0.401 ± 0.026
650	224.12 ± 13.24	190.89 ± 7.41	1.195 ± 0.288	0.887 ± 0.085
750	94.88 ± 6.48	81.41 ± 6.69	0.541 ± 0.063	0.376 ± 0.025
850	14.33 ± 0.86	10.42 ± 2.24	0.161 ± 0.021	0.047 ± 0.013
950	10.83 ± 0.77	7.12 ± 1.86	0.147 ± 0.024	0.032 ± 0.009

of O-, N-, and S-containing structures, which tend to have high Raman scattering ability (Li et al., 2006). The increases in the ratio of the peak intensity of the D-band to that of the G-band (I_D/I_G ratio) at temperatures of 450–750 °C indicate the relative increases in the concentrations of aromatic rings having six or more fused benzene rings, derived from both the dehydrogenation of hydroaromatics and the growth of aromatic rings in the char during pyrolysis. At temperatures higher than 750 °C, the I_D/I_G ratios showed relatively slight decreases with increase the temperature, and this indicated that additional large (more than six fused benzene rings) aromatic ring systems were produced by further ring condensation at high temperatures (Li et al., 2006; Wu et al., 2009). As shown in Table 1, the G_R, V_L, and V_R bands represent the amorphous structures, especially those relatively small aromatic ring systems possessing 3–5 fused benzene rings. Consequently, the band-area ratio between the D band and the combined $G_R + V_L + V_R$ band can measure the ratio between the large (>6 rings) and relatively small aromatic ring systems. The increasing trend of the band-area ratio between the D band and the combined $G_R + V_L + V_R$ band signifies that these relatively small aromatic sing systems are converted to the large aromatic ring systems with increase in the temperature (Li et al., 2006; Wu et al., 2009).

The specific surface area and pore volume of the solid products at varied temperatures are shown in Table 5. To describe the detailed evolution of the internal pore characteristics during pyrolysis, a pore-size distribution profile was obtained based on the DFT, and the results are shown in Fig. 4. The classification of micro-, meso-, and macropores follow the standards of International Union of Pure and Applied Chemistry, which prescribes that micropores have sizes less than 2 nm, macropores are larger than 50 nm, and the mesopores range from 2 to 50 nm (Feng and Bhatia, 2003).

The surface area of raw cotton stalk is 2.19 cm^2/g, while the outer surface area (calculated by particle size and density) is only 0.02 m^2/g. In the raw cotton stalk, there are many channel pores generated for the mass transmission during the growth process as a plant and the pores size were mesopore and macropore since no micropore was observed (shown in Fig. 4a). Therefore, these meso- and macropore would be beneficial to volatile precipitation. Compared with raw cotton stalk, the release of approximately 30% of the mass as volatile matter (as shown in Fig. 1) only enlarged the surface area of chars at 250 °C to a small extent, and the surface area only increases to 3.02 m^2/g, which may be due to the degradation of the hemicellulose because the hemicellulose has a high reactivity during thermal treatment at lower temperature (Chen and Kuo, 2011) and the degradation reaction of hemicelluloses occurs with low enthalpy change (Ibbett et al., 2011). The result of XRD analysis also indicates that the cellulose is not degraded since there is no significant change for the broad peaks at 16° and 22°. However, the pore-size distribution had a significant change—some micropores were generated, which became the major type of pores (more than 80%), instead of the majority of mesopores found in raw cotton stalk. The disappearance of these mesopores might be attributed to the following: mesopores in the raw sample are composed of hemicellulose; and the generation of micropores might be caused by the rupture of the hemicellulose along with other organic compounds.

Continuous increase in the temperature up to 450 °C results a major increase of the surface area focused around the pores of sizes 1.2 and 1.0 nm, but these increased micro pores only causes slight increasing of surface area from 3.02 to 7.96 m^2/g. Several researchers suggest that the degradation of cellulose is occurring during 250–450 °C (Shen and Gu, 2009; Vamvuka and Sfakiotakis, 2011; Yang et al., 2006b), and the result form the releasing of gas and liquid product also indicates the cellulose has decomposed. The result of XRD analysis shows that the crystal structure of cellulose is destroyed and some amorphous carbon structure such as 3–6 fused ring structure is present. It is suggested that the micropore may be constructed by these amorphous carbon structure, but it is difficult to identify these small amount of amorphous structure is derived from the decomposition of whether cellulose or lignin because the decomposition of lignin also occurs in this temperature range (Vamvuka and Sfakiotakis, 2011; Yang et al., 2006b, 2007).

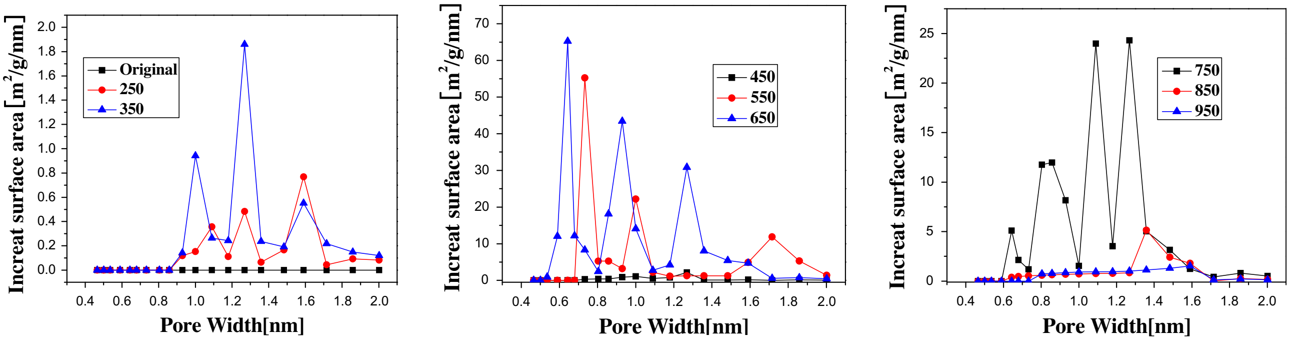

(a) micro pores (<2nm)

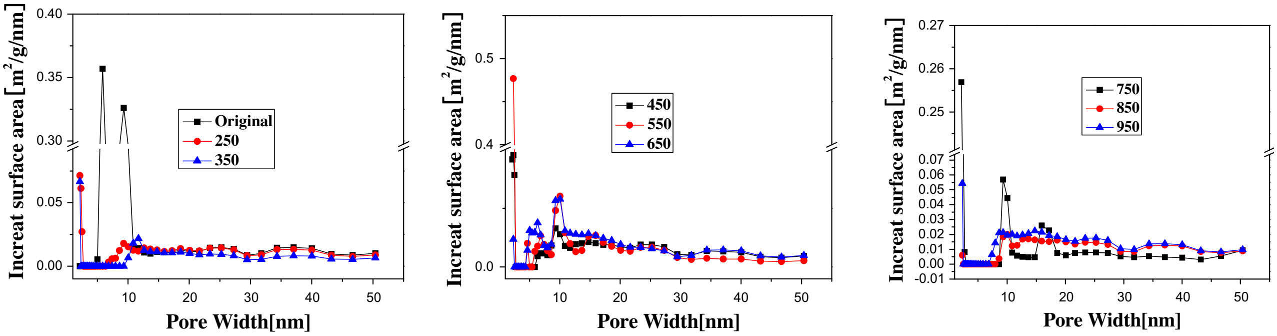

(b) meso pore (2-50nm)

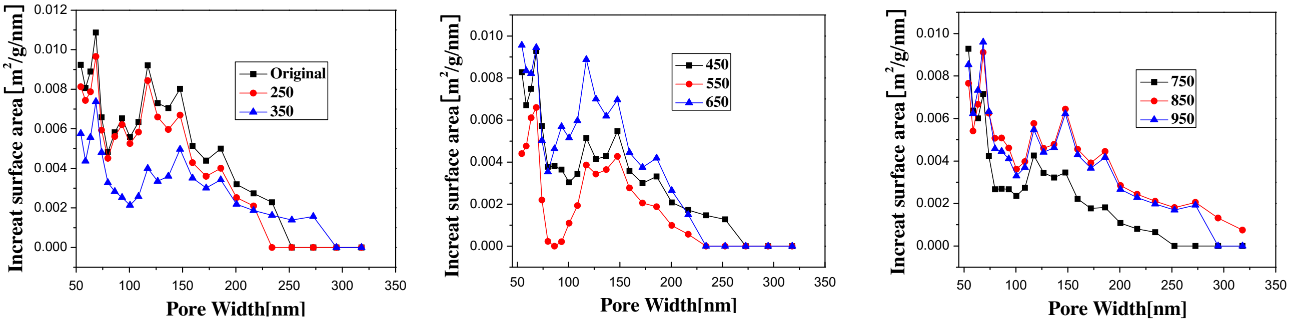

(c) macro pore (>50nm)

Fig. 4. Pore size distribution (nm) of cotton stalk and the chars obtained at different temperature by DFT analysis.

However, with the temperature increasing further to 550 °C, a significant increase of the surface area at the pores of sizes 0.73 and 1.0 nm is found, causing the total surface area to increase from 7.96 to 122.92 m^2/g. This increase may be attributed to the decomposition of lignin and the quick release of H_2 and CH_4 at this temperature. At 650 °C, further degradation of lignin and the reaction of aromatic condensation continually generate more micropores. The result from XRD and Raman analysis all indicate that the amount of amorphous carbon structure are up to the maximum during 450–650 °C, and the micro surface area was focus on the pore of sizes 0.62, 0.73, 0.9 and 1.0 nm but these pore sizes is not the characteristic pore existing in the graphite (Feng and Bhatia, 2003). It implies that the amorphous structures possessing 3–10 fused benzene rings (shown in Raman analysis) might be constructed these special micro pores.

But with the temperature increasing further to 950 °C, a blockade of the micropores is detected, which might be due to the plasticity of solid charcoal and the release of tar. In additional, the results of XRD and Raman analysis shows that the microcrystalline structure of graphite is present in the chars at high temperature, therefore, the process that the amorphous carbon structure converts to graphite microcrystalline structure might cause the decrease of surface area, which strongly proved that the good porosity is attributed to the amorphous carbon structure the same as the studies reported by Fu et al. (2011) and Liu et al. (2011). In this study, the pyrolysis process was a slow pyrolysis and the retention time of chars in the reactor was up to 30 min longer than these fast pyrolysis, therefore, the value of surface area of chars especially obtained at 550–650 °C was up to 200 m^2/g, which is larger than several previous work (Fu et al., 2011; Liu et al., 2011).

For the biomass-based polygeneration system, a dramatic economical profitability can be obtained from the charcoal, which has a widespread utilization and a huge demand from the consumer. First, the charcoal could be used as a fuel, instead of charcoal from the forest wood-carbonization industry, to reduce the destruction of forests. Second, a good-quality charcoal has a high calorific value and lower amount of volatiles. As Table 4 shows, to obtain a good fuel-grade charcoal, the operating temperature should be more than 550 °C. Moreover, the optimum temperature should be about 550–650 °C, which can yield the best charcoal using the least cost in terms of energy. The charcoal obtained can also be used as an adsorbent because of the good pore characteristics, as shown in Fig. 4 and Table 5. And the best condition for operation is 550–650 °C.

4. Conclusion

The evolution of product characteristics could be good explaining the process mechanism of biomass pyrolysis. A relationship between the pore distribution of solid products and the fused aromatic rings system revealed by Raman analysis might be exist, and a further study should be perform to quantify this relationship. A range of 550–750 °C was considered as the optimum operating temperature of Biomass-Based Pyrolytic Polygeneration. The calorific value of the charcoal achieved is approximately 28 MJ/kg, and the surface area is greater than 200 m^2/g. Meanwhile, the calorific value of the gas obtained reaches 8–9 MJ/m^3.

Acknowledgements

The authors wish to express the great appreciation of the financial support from National Nature Science Foundation of China (50930006, 50806027, 51021065 and 51076058) and The National Key Technology R&D Program (2011BAD15B05) and the technical support from Analytical and Testing Center in Huazhong University of Science & Technology (http://atc.hust.edu.cn).

Appendix A. Supplementary data

Supplementary data associated with this article can be found, in the online version, at doi:10.1016/j.biortech.2011.10.074.

References

Ayhan, D., 2007. The influence of temperature on the yields of compounds existing in bio-oils obtained from biomass samples via pyrolysis. Fuel Process. Technol. 88, 591–597.

Bahng, M.K., Mukarakate, C., Robichaud, D.J., Nimlos, M.R., 2009. Current technologies for analysis of biomass thermochemical processing: a review. Anal. Chim. Acta 651, 117–138.

Chen, W.H., Kuo, P.C., 2011. Torrefaction and co-torrefaction characterization of hemicellulose, cellulose and lignin as well as torrefaction of some basic constituents in biomass. Energy 36, 803–811.

China NDaRCo, 2010. The statistic table on the temporary subsidy for electricity price to the direct burning power generate using stalks during January to June at 2010. <http://www.sdpc.gov.cn/zfdj/jggg/dian/W020110215346202706689.pdf> (15.02.2011)

Demiral, İ, Ayan, E.A., 2011. Pyrolysis of grape bagasse: effect of pyrolysis conditions on the product yields and characterization of the liquid product. Bioresour. Technol. 102, 3946–3951.

Duman, G., Okutucu, C., Ucar, S., Stahl, R., Yanik, J., 2011. The slow and fast pyrolysis of cherry seed. Bioresour. Technol. 102, 1869–1878.

Feng, B., Bhatia, S.K., 2003. Variation of the pore structure of coal chars during gasification. Carbon 41, 507–523.

Fu, P., Hu, S., Xiang, J., Sun, L.S., Li, P.S., Zhang, J.Y., Zheng, C.G., 2009a. Pyrolysis of maize stalk on the characterization of chars formed under different devolatilization conditions. Energy Fuels 23, 4605–4611.

Fu, P., Hu, S., Sun, L.S., Xiang, J., Yang, T., Zhang, A.C., Zhang, J.Y., 2009b. Structural evolution of maize stalk/char particles during pyrolysis. Bioresour. Technol. 100, 4877–4883.

Fu, P., Yi, W.M., Bai, X.Y., Li, Z.H., Hu, S., Xiang, J., 2011. Effect of temperature on gas composition and char structural features of pyrolyzed agricultural residues. Bioresour. Technol. 102, 8211–8219.

Ibbett, R., Gaddipati, S., Davies, S., Hill, S., Tucker, G., 2011. The mechanisms of hydrothermal deconstruction of lignocellulose: new insights from thermal–analytical and complementary studies. Bioresour. Technol. 102, 9272–9278.

Ismadji, S., Sudaryanto, Y., Hartono, S.B., Setiawan, L.E.K., Ayucitra, A., 2005. Activated carbon from char obtained from vacuum pyrolysis of teak sawdust: pore structure development and characterization. Bioresour. Technol. 96, 1364–1369.

Keown, D.M., Li, X.J., Hayashi, J., Li, C.Z., 2008. Evolution of biomass char structure during oxidation in O(2) as revealed with FT-Raman spectroscopy. Fuel Process. Technol. 89, 1429–1435.

Laird, D.A., Brown, R.C., Amonette, J.E., Lehmann, J., 2009. Review of the pyrolysis platform for coproducing bio-oil and biochar. Biofuels Bioprod. Biorefin. 3, 547–562.

Li, X.J., Hayashi, J., Li, C.Z., 2006. FT–Raman spectroscopic study of the evolution of char structure during the pyrolysis of a Victorian brown coal. Fuel 85, 1700–1707.

Liu, H., Jiang, G.M., Zhuang, H.Y., Wang, K.J., 2008. Distribution, utilization structure and potential of biomass resources in rural China: with special references of crop residues. Renew. Sustainable Energy Rev. 12, 1402–1418.

Liu, P., Pistikopoulos, E.N., Li, Z., 2010. A multi-objective optimization approach to polygeneration energy systems design. AIChE J. 56, 1218–1234.

Liu, W.J., Zeng, F.X., Jiang, H., Zhang, X.S., 2011. Preparation of high adsorption capacity bio-chars from waste biomass. Bioresour. Technol. 102, 8247–8252.

Mahinpey, N., Murugan, P., Mani, T., Raina, R., 2009. Analysis of bio-oil, biogas, and biochar from pressurized pyrolysis of wheat straw using a tubular reactor. Energy Fuels 23, 2736–2742.

Sevgi, Ş., 2003. Slow pyrolysis of wood barks from *Pinus brutia* Ten. and product compositions. Bioresour. Technol. 89, 307–311.

Shangguan, J., Miao, M.Q., Chang, L.P., Li, F., Xie, K.C., 2010. Desulfurization matching with coal poly-generation system based on dual gas resources. Fuel 89, 833–837.

Shen, D.K., Gu, S., 2009. The mechanism for thermal decomposition of cellulose and its main products. Bioresour. Technol. 100, 6496–6504.

Vamvuka, D., Sfakiotakis, S., 2011. Effects of heating rate and water leaching of perennial energy crops on pyrolysis characteristics and kinetics. Renew. Energy 36, 2433–2439.

Venderbosch, R.H., Prins, W., 2010. Fast pyrolysis technology development. Biofuels Bioprod. Biorefin. 4, 178–208.

Wang, Z.Y., Cao, J.Q., Wang, J., 2009. Pyrolytic characteristics of pine wood in a slowly heating and gas sweeping fixed-bed reactor. J. Anal. Appl. Pyrolysis 84, 179–184.

Wang, S., Guo, X., Wang, K., Luo, Z., 2011. Influence of the interaction of components on the pyrolysis behavior of biomass. J. Anal. Appl. Pyrolysis 91, 183–189.

Wu, H.W., Yip, K., Tian, F.J., Xie, Z.L., Li, C.Z., 2009. Evolution of char structure during the steam gasification of biochars produced from the pyrolysis of various mallee biomass components. Ind. Eng. Chem. Res. 48, 10431–10438.

Yang, H.P., Yan, R., Chen, H.P., Lee, D.H., Liang, D.T., Zheng, C.G., 2006a. Mechanism of palm oil waste pyrolysis in a packed bed. Energy Fuels 20, 1321–1328.

Yang, H.P., Yan, R., Chen, H.P., Zheng, C.G., Lee, D.H., Liang, D.T., 2006b. In-depth investigation of biomass pyrolysis based on three major components: hemicellulose, cellulose and lignin. Energy Fuels 20, 388–393.

Yang, H.P., Yan, R., Chen, H.P., Lee, D.H., Zheng, C.G., 2007. Characteristics of hemicellulose, cellulose and lignin pyrolysis. Fuel 86, 1781–1788.

Yang, Y.L., Zhang, P.D., Zhang, W.L., Tian, Y.S., Zheng, Y.H., Wang, L.S., 2010. Quantitative appraisal and potential analysis for primary biomass resources for energy utilization in China. Renew. Sustainable Energy Rev. 14, 3050–3058.

Yao, Y., Gao, B., Inyang, M., Zimmerman, A.R., Cao, X., Pullammanappallil, P., Yang, L., 2011. Biochar derived from anaerobically digested sugar beet tailings: characterization and phosphate removal potential. Bioresour. Technol. 102, 6273–6278.

Zhang, P.D., Yang, Y.L., Tian, Y.S., Yang, X.T., Zhang, Y.K., Zheng, Y.H., Wang, L.S., 2009. Bioenergy industries development in China: dilemma and solution. Renew. Sustainable Energy Rev. 13, 2571–2579.